KSCE Journal of Civil Engineering (2021) 25(2):516-528
DOI 10.1007/s12205-020-2056-0

pISSN 1226-7988, eISSN 1976-3808
www.springer.com/12205

Structural Engineering

Stiffness Assessment of Cracked Reinforced Concrete Beams Based on a Fictitious Crack Model

Chunyu Fu[a], **Yin Zhu**[a], **and Dawei Tong**[a]

[a]*Dept. of Civil and Transportation Engineering, Hohai University, Nanjing 210098, China*

ARTICLE HISTORY

Received 12 November 2019
Revised 23 April 2020
Accepted 13 September 2020
Published Online 30 November 2020

KEYWORDS

Reinforced concrete beams
Fictitious crack
Beam stiffness
Nonlinear stress
Force equilibrium

ABSTRACT

A fictitious crack model is introduced into cracked reinforced concrete beams to assess the changing beam stiffness under loads. Firstly, nonlinear concrete stress distributions near cracks are built based on the model. Then the stress of the steel bar at the cracked section is considered as cohesive stress. The concrete and steel stresses are substituted into the equilibrium equations of forces to solve the concrete stress. Based on the solution, the section inertias are estimated by iterating the calculation of the cracking open displacement, and finally the beam stiffness is assessed. Experimental data from seven concrete beams after cracking are adopted to validate the effectiveness of the proposed method, and the results show that the fictitious cracks ahead of actual cracks increase their depth with the load, which will raise the neutral axis and change the inertias of cracked sections and their neighboring sections. These changes are taken into account in the stiffness assessment, so the results predicted by the proposed method are shown to coincide well with the nonlinear deflections measured in the experiments.

1. Introduction

Deflection control is an important objective in the design of reinforced concrete beams. However, the concrete in these beams is easy to crack due to its low tensile strength, which has a great effect on the beam stiffness through altering the bearing area of cross sections. So in recent decades, how to assess the stiffness of cracked concrete beams became a hot topic of civil engineering.

The effective inertia of cross sections was early proposed for the stiffness control of the cracked reinforced concrete beams in design. Branson (1965) proposed a model for the effective inertia using a weighted average of the fully cracked inertia and the uncracked inertia. But the comparison with experimental data showed that the instantaneous deflections of reinforced concrete beams and slabs after cracking were underestimated in Branson's model (Gilbert, 2007; Gribniak et al., 2013). Bischoff (2005) developed Branson's model by using empirical parameters that decrease the ratio of the uncracked inertia to the cracked inertia, which was suggested by the fib Model Code (CEB-FIP, 2012). Kalkan and Lee (2013) compared these models, and found that Bischoff's model produced more conservative results for heavily-reinforced concrete beams. These models relied on the empirical parameters to obtain the effective inertia, and do not take the actual cracking pattern of reinforced concrete beams into account. Therefore, they just can be applied in the design stage.

To take the effects of cracking pattern on the structural serviceability into account, François et al. (2006) put forward a macro-finite-element (MFE) method to estimate a homogenized average section inertias according to the measurement of a transfer length. Castel et al. (2012) modified the MFE method by assuming the distribution of steel and concrete strains in the cracked span, which was conditioned by using the cracking moment and maximum moment. Castel et al. (2014) further considered the simultaneous effects of cracks and damage on the bond through introducing a damage parameter D_{ccc}. Murray et al. (2016) considered the historical loading in Castel et al.'s method to study the creep and shrinkage effects on the beam stiffness. Xu et al. (2018) modified the damage variable D_{ccc} by using the creep and shrinkage coefficients in the assessment of the time-dependent stiffness.

In these existing methods, the concrete was taken as an elastic material, and exact cracking patterns including the crack depth were not considered, so the concrete stress near the crack tip was

CORRESPONDENCE Chunyu Fu fuyupiece@163.com Dept. of Civil and Transportation Engineering, Hohai University, Nanjing 210098, China

ⓒ 2021 Korean Society of Civil Engineers

not analyzed, and the beam stiffness was roughly estimated. In fact, as a quasi-brittle material, the concrete has a nonsingular stress field near the crack tip, and possesses many micro-cracks ahead of the tip (Wittmann, 1983). Before the crack propagation, the concrete structure will exhibit a certain degree of nonlinearity due to these micro-cracks (Hu and Duan, 2010), which finally affects the structural stiffness. Many fracture models have been built to study this nonlinearity. As one of these models, the fictitious crack model can preferably describe the stress state near the concrete crack (Hillerborg et al., 1976), and has been widely used in the analysis of concrete crack propagation and structural bearing capacity (Choubey et al., 2016; Fayyad and Lees, 2018; Qing and Cheng, 2018).

To estimating the nonlinear deflection of the reinforced concrete beams, the fictitious crack model is introduced into the assessment of the beam stiffness in this paper. Firstly, nonlinear concrete stress distributions near cracks are built based on the model. Then the stress of the steel bar at the cracked section is considered as cohesive stress. The concrete and steel stresses are substituted into the equilibrium equations of forces to precisely solve the concrete stress. Based on the solution, the section inertias are estimated by iterating the calculation of the cracking open displacement, and finally the beam stiffness is assessed.

2. Assessment Methodology

2.1 Nonlinear Stress Distributions of Cracked Sections

A reinforced concrete beam after cracking is considered, and its span, height and width are respectively L, h and b, as shown in Fig. 1. It is assumed that all the cracks do not propagate in the stiffness assessment. The beam is subjected to four-point bending. The concrete stress of the section where the Crack I with an initial depth of a_0 is located is studied firstly.

A fictitious crack is modeled to be located ahead of the Crack I, and its depth is a_f. The stress at the fictitious crack tip is taken as the flexural tensile strength f_{ct} of concrete (Wu et al., 2006). The distribution of the concrete strains ahead of the tip is assumed to be linear along the beam height (Wu et al., 2006). The relationship between the concrete stress and strain is almost linear, so the stress distribution along with the height from the extreme compression fibers to the tip of the fictitious crack as shown in Fig. 2.

In the fictitious crack, concrete cohesive stresses σ_w are present, and their values are obtained according to the expression proposed by Reinhardt et al. (1986), which is a function of the fictitious crack opening displacement w_f.

$$\sigma_w = f_{ct}\left[\left(1+\frac{c_1^3}{w_0^3}w_f^3\right)e^{-\frac{c_2}{w_0}w_f} - \frac{(1+c_1^3)e^{-c_2}}{w_0}w_f\right], \tag{1}$$

where c_1 and c_2 are two material constants, w_0 is the maximum width of crack opening when σ_w becomes 0. The crack surface is assumed to remain plane (Wu et al., 2006), so the crack opening displacement changes linearly along the height at the crack surface, and can be expressed as

$$w_f = \frac{(a_f + a_0 - y)}{a_f + a_0}w_b \quad (a_0 \le y \le a_0 + a_f), \tag{2}$$

where w_b is the crack opening displacement at the beam bottom.

If an initial value is given for w_b, the concrete cohesive strain can be obtained by Eq. (2). The steel stress σ_t is also regarded as a function of w_b in this paper, and its calculation will be introduced in Section 2.3. Meanwhile, a_f can be expressed based on the strain distribution ahead of the fictitious crack tip.

$$a_f = y_n - f_{ct}\frac{h-y_n}{\sigma_{ct}}. \tag{3}$$

where y_n is the y-axis coordinate of section neutral axis, and σ_{ct} denotes the concrete stress at the beam top.

As a result, there are two unknowns in the stress distribution shown in Fig. 2: the neutral axis location y_n and the top stress σ_{ct}.

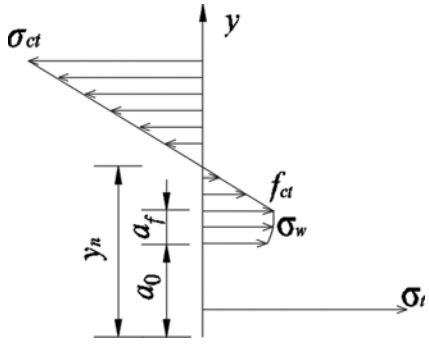

Fig. 2. Stress Distribution of the Cracked Section

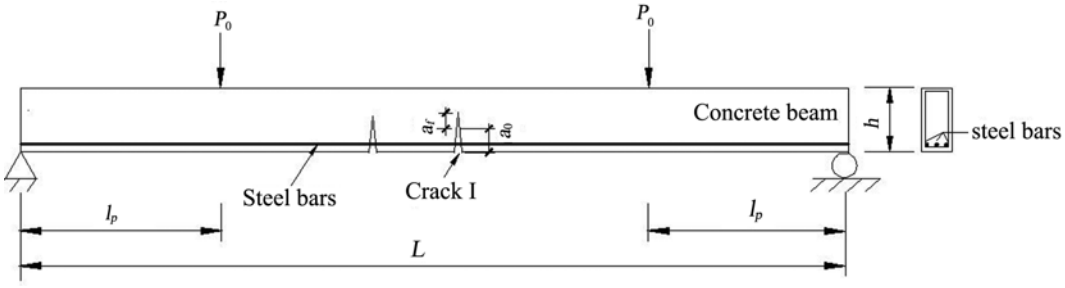

Fig. 1. Layout of the Reinforced Concrete Beam with Distributed Cracks

The internal forces and moments are equilibrated for the cracked section, so they can be adopted to solve these unknowns.

$$\int_{A_c} \sigma_c(y)\mathrm{d}A + \sigma_t A_t = 0 \,, \tag{4}$$

$$\int_{A_c} \sigma_c(y)(y - y_n)\mathrm{d}A + \sigma_t A_t (y_n - d_t) = M_0 \,, \tag{5}$$

where A_c and A_t are the concrete and steel areas, respectively, σ_c denotes the concrete stress distribution along the beam height, and d_t is the distance from the steel centroid to the beam bottom.

By substituting the stress distribution into Eqs. (4) and (5), the following equations are obtained:

$$\int_{A_{ca}} \sigma_{ct} \frac{(y - y_n)}{h - y_n}\mathrm{d}A + \int_{A_{cf}} \sigma_w(y)\mathrm{d}A + \sigma_t A_t = 0 \,, \tag{6}$$

$$\int_{A_{ca}} \sigma_{ct} \frac{(y - y_n)^2}{h - y_n}\mathrm{d}A + \int_{A_{cf}} \sigma_w(y)(y - y_n)\mathrm{d}A + \sigma_t A_t (y_n - d_t) = M_0 \,, \tag{7}$$

where A_{ca} denotes the concrete area above the fictitious crack, and A_{cf} is the area between the tips of the fictitious and actual cracks. Eqs. (6) and (7) are a set of simultaneous equations, and through solving them, the two unknowns, σ_{ct} and y_n, are obtained.

If the load is small or the steel force is large, the bending moment acting on the concrete is small. So the stress σ_{ctp} at the crack tip may not reach the flexural tensile strength f_{ct}, and the fictitious crack may not appear. In such a case, the stress distributions ahead of the crack tip are also assumed to be linear, and Eqs. (6) and (7) will be changed into the following equations.

$$\int_{A_{cu}} \sigma_{ct} \frac{(y - y_n)}{h - y_n}\mathrm{d}A + \sigma_t A_t = 0 \tag{8}$$

$$\int_{A_{cu}} \sigma_{ct} \frac{(y - y_n)^2}{h - y_n}\mathrm{d}A + \sigma_t A_t (y_n - d_t) = M_0 \tag{9}$$

If the cross section is a rectangular section, Eqs. (8) and (9) can be further simplified as follows:

$$-\sigma_{ct}(h - y_n)b/2 + \sigma_{ct} b(y_n - d_c)^2/[2(h - y_n)] + \sigma_t A_t = 0 \,, \tag{10}$$

$$\sigma_{ct}(h - y_n)^2 b/3 + \sigma_{ct} b(y_n - d_c)^3/[3(h - y_n)] + \sigma_t A_t (y_n - d_t) = M_0 \,. \tag{11}$$

2.2 Nonlinear Stress Distributions of Uncracked Sections

The crack occurrence doesn't only change the stress distribution at the cracked section, but also cause nonlinear strain distribution at sections near the crack. The region affected by the crack can be regarded as a region where the tensile force of the steel bars is transferred to the concrete by the bond stress (Castel et al., 2012). If the transfer length l_t is defined as a distance from the crack to the first point where the steel and concrete strains are equal to each other, the length l_r of the entire effect region is equal to $2l_t$. According to the fib Model Code 2010 (CEB-FIP, 2012), l_t can be estimated as follows:

$$l_t = c + \frac{f_{ctm} D_s}{4\tau_{bms}\rho_{ef}} \,, \tag{12}$$

where c denotes the concrete cover thickness, f_{ctm} is the mean tensile strength of concrete, D_s is the diameter of steel bars, ρ_{ef} denotes the reinforcement ratio, and τ_{bms} is the strength of steel-concrete bond; for the stabilized cracking stage, $\tau_{bms} = 1.8 f_{ctm}$.

The bond stress $\tau(x)$ can be assumed to be linear according to the model proposed by Castel et al. (2012), and the concrete stress near the bottom is second-degree polynomial. In this paper, the bottom stress is also assumed to be a second-degree polynomial function in the effect region, and is given by

$$\sigma_{cb}(x) = \sigma_{cb0} g(x) \,, \tag{13}$$

$$g(x) = \frac{4x}{l_r} - \frac{4x^2}{l_r^2} \qquad (0 \le x \le l_r/2) \,, \tag{14}$$

where the x-axis coordinate origin is located at the cracked section. The stress distribution is assumed to be symmetrical to the crack. σ_{cb0} is the bottom strain of sections unaffected by cracks, and obtained by adopting the classical beam theory

$$\sigma_{cb0} = \frac{M_0}{I_0} y_n \,, \tag{15}$$

where I_0 denotes the section inertia unaffected by cracks, including the steel contribution.

If the spacing l_s between two adjacent cracks is less than $2l_t$, sections between the adjacent two cracks are regarded to be influenced solely by the crack closer to them. The length l_r of the region affected by one crack is equal to $(l_{sl} + l_{sr})/2$, where l_{sl} and l_{sr} denote the left and right crack spacings, respectively.

Then the stress distribution along the section height is considered. Due to the crack effects, the stresses are no longer linear along the height in the effect region. A nonlinear model shown in Fig. 3 is adopted to simulate the stress distribution. An inflection point is assumed to occur at the position whose height is identical with that of the fictitious crack tip, as the crack occurrence causes two different stress distributions of the parts above and below the crack tip. The stresses of the above part keep linear along the height, while the stresses of the below part

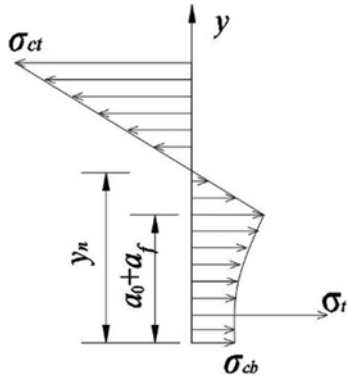

Fig. 3. Stress Distribution of Sections in the Effect Region

follow a nonlinear distribution, which can be expressed as

$$\sigma_c(y)=\left(\sigma_{ct}\frac{a_0+a_f-y_n}{h-y_n}-\sigma_{cb}\right)\left(\frac{y}{a_0+a_f}\right)^{\eta}+\sigma_{cb}\qquad y\le a_0+a_f\,, \tag{16}$$

where the parameter η denotes the nonlinear distribution, and here is assumed to be related to the rate of σ_{cb0} to σ_{cb}

$$\eta=\mathrm{int}(\sigma_{cb0}/2\sigma_{cb})\,, \tag{17}$$

where int( ) denotes an algorithm that a number is rounded to the nearest integer.

By substituting this stress distribution into the equilibria Eqs. (4) and (5), the following equations are gotten:

$$\int_{A_{cu}}\sigma_{ct}\frac{(y-y_n)}{h-y_n}\mathrm{d}A+\int_{A_{cb}}\left(\sigma_{ct}\frac{a_0+a_f-y_n}{h-y_n}-\sigma_{cb}\right)\left(\frac{y}{a_0+a_f}\right)^{\eta}+\sigma_{cb}+\mathrm{d}A+\sigma_tA_t=0, \tag{18}$$

$$\int_{A_{cu}}\sigma_{ct}\frac{(y-y_n)^2}{h-y_n}\mathrm{d}A+\int_{A_{cb}}\left[\left(\sigma_{ct}\frac{a_0+a_f-y_n}{h-y_n}-\sigma_{cb}\right)\left(\frac{y}{a_0+a_f}\right)^{\eta}+\sigma_{cb}\right](y-y_n)\mathrm{d}A+\sigma_tA_t(d_t-y_n)=M_0, \tag{19}$$

where A_{cb} and A_{cu} denote the concrete areas of the parts below and above the inflection point. Through the solution of Eqs. (18) and (19), the top stress σ_{ct} and the neutral axis location y_n can be obtained.

2.3 Analysis of Strains Developed in Steel Reinforcement

If the bond stress $\tau(x)$ is assumed to be linear, the steel strains near the crack are given as (Castel et al., 2012)

$$\varepsilon_t(x)=\varepsilon_{t0}g(x)+\varepsilon_{tc}[1-g(x)]\,, \tag{20}$$

where ε_{tc} is the steel strain at the cracked section, and ε_{t0} is the steel strain at the sections unaffected by the cracks, which is calculated by the classical beam theory

$$\varepsilon_{t0}=\frac{M_0}{E_cI_0}(y_n-d_t)\,, \tag{21}$$

where E_c is the concrete elastic modulus.

The strain ε_{tc} is regarded to be related to the crack opening displacement, so this opening displacement is analyzed firstly. From the strain distributions of the steel bar and concrete, the crack opening displacement w_t at the steel level can be defined as the total difference in elongations between the steel and concrete measured over the entire length of the region affected by the crack, so w_t can be expressed as

$$w_t=\int_{-l_r/2}^{l_r/2}\Delta\varepsilon(x)\mathrm{d}x\,, \tag{22}$$

where $\Delta\varepsilon(x)$ is equal to $(\varepsilon_t-\varepsilon_{ct})$, and ε_t and ε_{ct} are the steel and concrete strains at the level of the steel, respectively.

ε_{ct} is considered to be quadratic nonlinear (Castel et al., 2012), and can be written as

$$\varepsilon_{ct}(x)=\varepsilon_{ct0}g(x)\,, \tag{23}$$

where ε_{ct0} is the concrete strain at the steel level at the sections unaffected by cracks. ε_{ct0} is equal to ε_{t0} at these sections. Therefore, $\Delta\varepsilon(x)$ can be expressed as

$$\Delta\varepsilon(x)=[1-g(x)]\varepsilon_{tc}\,, \tag{24}$$

So $\Delta\varepsilon$ is related to the strain ε_{tc}. Then Eq. (24) is substituted into Eq. (22), the strain ε_{tc} can be expressed as

$$\varepsilon_{tc}=w_t/\int_{-l_r/2}^{l_r/2}[1-g(x)]\mathrm{d}x\,, \tag{25}$$

w_t can be obtained through the relationship between the cracking open displacements.

$$w_t=\frac{w_b}{d_c+d_f}(d_c-d_t) \tag{26}$$

Therefore, the steel strain ε_{tc} is obtained through Eqs. (25) and (26), and the steel stress at the cracked section can be viewed as a cohesive stress, which is related to the cracking open displacement. The steel strains in the effect region are calculated through Eq. (20), and the steel stress can be calculated by using the linear relationship between the strain and stress.

2.4 Calculation of Inertias

Although the concrete stress distribution is affected by the cracks, according to the stress distribution models in Figs. 2 and 3, it still changes linearly from the section top to the neutral axis. Therefore, the cracked beam can be viewed as a beam whose strains meet the plane-section assumption when the geometric characteristics can be calculated, and the section inertia I_{eq} can be expressed using the stress at the beam top and the location of the neutral axis.

$$I_{eq}=\frac{M_0}{\sigma_{ct}}(h-y_n) \tag{27}$$

Similarly, the elongation of the beam bottom caused by the crack also can be expressed as

$$\Delta l_b=\int_{-l_r/2}^{l_r/2}\frac{\sigma_{ct}(x)/E_c}{h-y_n(x)}y_n(x)\mathrm{d}x\,. \tag{28}$$

The cracking open displacement at the bottom can be considered as the difference between the elongation and deformation of the bottom, which is expressed as

$$w_b=\Delta l_b-\int_{-l_r/2}^{l_r/2}\sigma_{cb}(x)/E_c\mathrm{d}x\,. \tag{29}$$

This calculated result can be used to update the initial value of the cracking open displacement at the bottom, which in turn affects the estimation of the concrete cohesive stress and the steel stress, and further the top stress and neutral axis. Therefore, the following iterative algorithm should be adopted to calculate the inertias of sections in the effect region:

1. Estimate an initial value of the cracking open displacement

at the bottom w_{bj} ($j = 0$).

2. Use w_{bj} to calculate the cracking open displacements at the location of the fictitious crack and the steel, and then the concrete cohesive stresses and the steel stresses are assessed through Eqs. (1) and (25), respectively.
3. Select key sections in the effect regions, and estimate their bottom stresses using Eq. (13); then build the stress distributions for the cracked section and key sections.
4. Use Eqs. (6) – (9) or Eqs. (18) and (19) to calculate the top stresses and neutral axis location of cracked sections and key sections.
5. Use these top stresses and neutral axes to recalculate the cracking open displacement $w_{b(j+1)}$ at the bottom through Eq. (29).
6. Compare the latest cracking open displacement, and calculate whether they satisfy the following inequality.

$$\left\| w_{b(j+1)} - w_{bj} \right\| < \varepsilon \,, \tag{30}$$

where ε is a permissible error.

7. If Eq. (30) is valid, the cracking open displacement is set to be w_{bj}, and calculate the inertias of the cracked section and key sections using Eq. (27); otherwise, j is assigned to $j + 1$, and return Step (2) to recalculate.

After the determination of the inertias in the effect region, the varying curve of the section inertias along the beam span can be fitted through these inertias. The beam stiffness is analyzed by using the finite-element method, and the beam is considered to be composed of elements with four degrees (vertical displacement and rotation at each end). The local stiffness matrix of an element is expressed as

$$\mathbf{K}_{le} = \int_0^{l_{me}} \frac{E_c I_f(\xi)}{l_{me}^3} \left(\frac{\mathrm{d}^2 \mathbf{N}(\xi)}{\mathrm{d}\xi^2} \right)^T \frac{\mathrm{d}^2 \mathbf{N}(\xi)}{\mathrm{d}\xi^2} \mathrm{d}\xi \,, \tag{31}$$

where l_{me} denotes the element length, I_f is the fitted curve of the inertias, ξ is equal to $(x\text{-}x_{ml})/l_{me}$ where x_{ml} is the x-axis coordinate value of the left end in the element, and $\mathbf{N}$ is the Hermite interpolation function (Logan, 2007).

In order to obtain the global stiffness matrix $\mathbf{K}_b$ of the beam, the local stiffness matrices of all elements are assembled and the coefficients corresponding to the same location are added. By substituting the boundary condition and the external load vector $\mathbf{F}$ into the finite element equations, Eq. (32), the displacement vector $\mathbf{X}$ of the beam can be obtained:

$$\mathbf{K}_b \mathbf{X} = \mathbf{F} \,. \tag{32}$$

3. Experimental Validation

Two experimental validations are proposed. Firstly, experimental data from Castel et al. (2014) are used for the validation. Secondly, two simply supported beams with a span of 2.6 m were cast at Hohai University in Nanjing, and their behaviors after cracking were tested specifically for this study.

3.1 Experiment Performed by Castel et al. (2014)

Six simply supported beams with a span of 3.3 m were cast in this experiment, and their cross sections were rectangular sections with a height of 0.4 m and a width of 0.3 m. The layout of reinforced steel bars is shown in Fig. 4. The experimental data from five beams, labeled B1, B2, B3, B5 and B6, are used to test the proposed method.

The flexural tensile strength f_{ct} of the concrete was 3.5 MPa and the elastic modulus E_c was 33 GPa. The steel yield stress f_y was 500 MPa. According to existing findings about the fracture characteristics of concrete (Wu et al., 2006), the material constants c_1 and c_2 are set to be equal to 3 and 7, respectively, and w_0 is 160 μm.

As shown in Fig. 4, all the beams were subjected to four-point bending. The beams were cracked under a precracking load followed by a sustained load. The precracking load was applied at 28 days after casting, and then all the beams were subjected to the sustained load for 6 months. The cracking pattern was measured after the sustained loading (Xu et al., 2018), as shown in Fig. 5. In order to assess the beam stiffness after cracking, ten loading and unloading cycles were performed on each beam, and The load and midspan deflection were measured in each cycle.

From Fig. 5, it is observed that cracks in the test beams had curved shapes and were not vertical. To accurately evaluate the crack spacing, a method proposed by Gribniak et al. (2016) is used. The crack spacing in this method was taken as the average distance of adjacent point clusters, which was estimated using a clustering technique.

Meanwhile, if observed from either side of the beams, the cracks do not exhibit the same pattern. Therefore, the crack depth and spacing should be analyzed from the south and north sides, respectively, and the section inertias also should be assessed by using the proposed method from the two sides.

In order to illustrate the assessment process, the north side of the beam B1 is used as an example. The depth and estimated spacing of cracks in the north side of the beam B1 are shown in Table 1. Based on these depths and spacing, the models for

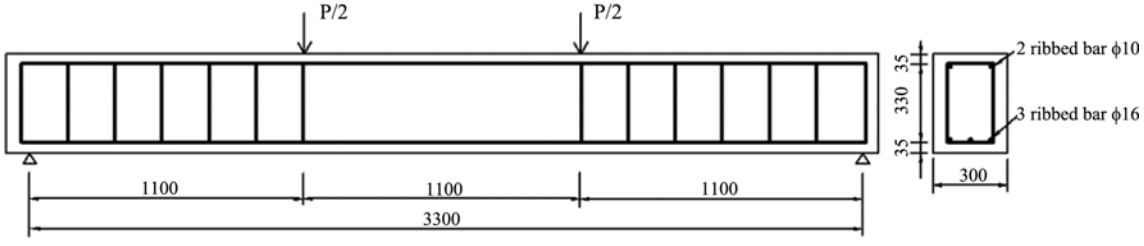

Fig. 4. Layout of Test Beams Constructed by Castel et al. (2014) (unit: mm)

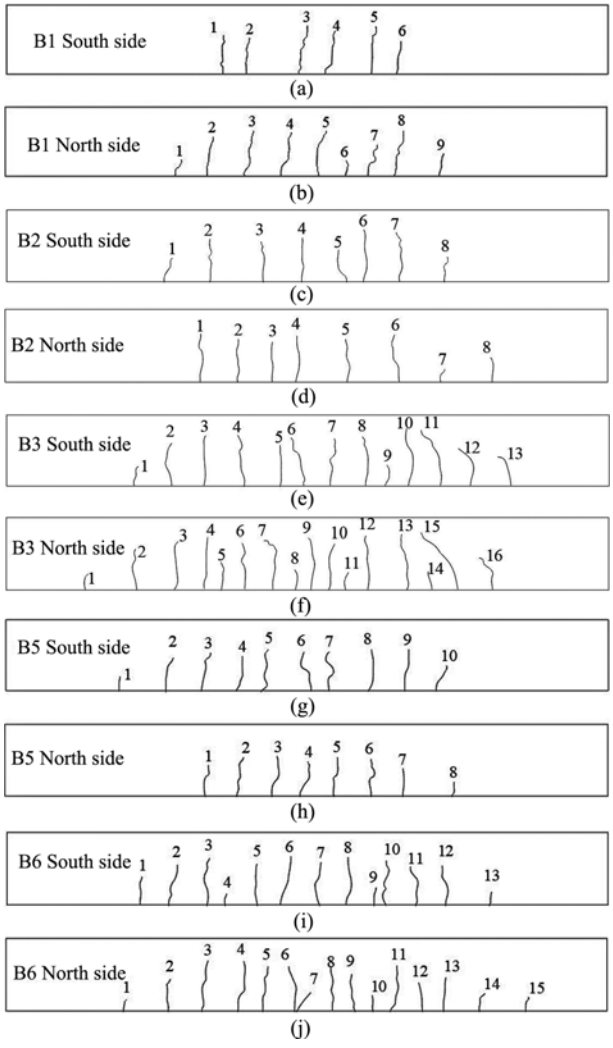

Fig. 5. Cracking Patterns of the Test Beams Provided by Xu et al. (2018): (a) B1 South Side, (b) B1 North Side, (c) B2 South Side, (d) B2 North Side, (e) B3 South Side, (f) B3 North Side, (g) B5 South Side, (h) B5 North Side, (i) B6 South Side, (j) B6 North Side

Table 1. The Measured Cracking Pattern for the North Side of the Beam B1 (unit: m)

Number	Location	Depth	Spacing
1	0.916	0.081	-
2	1.096	0.218	0.181
3	1.314	0.257	0.218
4	1.527	0.240	0.212
5	1.733	0.254	0.207
6	1.865	0.082	0.132
7	2.017	0.170	0.151
8	2.165	0.253	0.149
9	2.406	0.122	0.240

nonlinear stress distributions are built for the sections in the effect region. Based on the iterative solution of these models, the concrete stress and neutral axis of the sections are gotten and the

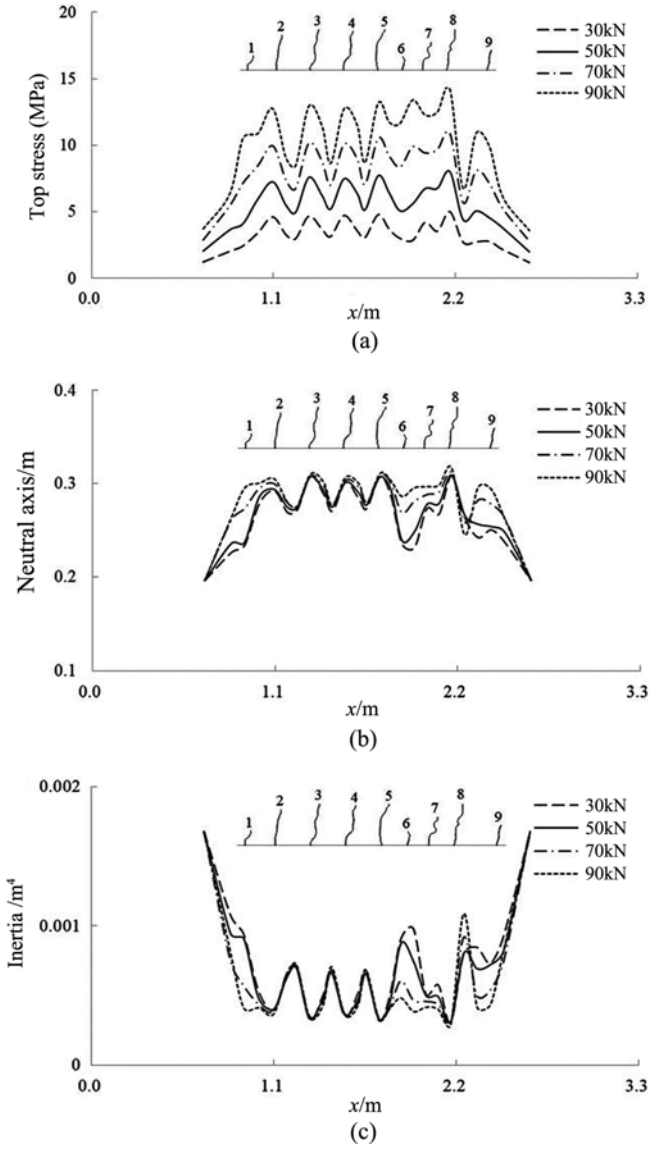

Fig. 6. Calculated Results in the Process of the Stiffness Assessment for the North Side of the Beam B1: (a) Top Strains, (b) Neutral Axes, (c) Inertias

inertias are estimated for the north side, as shown in Fig. 6.

From Fig. 6, it is found that the top stresses reach their local maximums at the location of every crack, while the neutral axes reach the local minimums. As a result, the inertias along the beam span are minimized at every crack. Besides, not only the stresses but also the neutral axes change when the load becomes large, so the section inertias will vary during the loading process, as shown in Fig. 6(c). The reasons for these changes may be found in Fig. 7.

Figure 7 takes some cracks in the beam B1 for examples to illustrate the changes of fictitious cracks and inertias. In these cracks, the depth of the 6th crack is smallest, and the 5th crack is deepest. It is observed that fictitious cracks ahead of the cracks with small depths change their depth obviously when the load becomes larger. This change causes a large variation in the

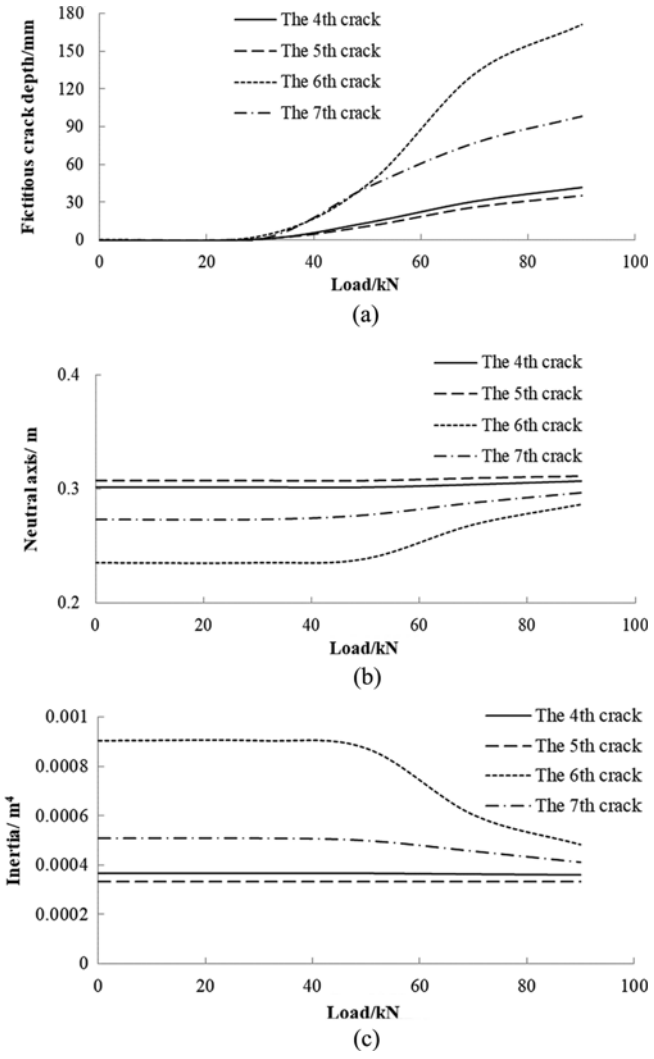

Fig. 7. Characteristics of Cracks in the North Side of the Beam B1: (a) The Fictitious Crack Depths, (b) The Neutral Axis of the Cracked Sections, (c) The Inertias of the Cracked Sections

neutral axis based on Eq. (3), and further affects the inertia of the cracked section, as shown in Figs. 7(b) and 7(c).

However, when the load is small, the depth of the fictitious cracks is equal to 0, as shown in Fig. 7(a). It is because the stress at the crack tip σ_{ctp} does not reach the flexural tensile strength f_{ct} under the small load, and the fictitious crack does not appear. Besides, under the large load, the depth of the fictitious crack ahead of a deep crack, such as the 6th crack, is also small. It may be due to the fact that the width of the deep crack is large under the large load, so the tensile force of the steel bars is large according to Eq. (20), and the tensile force of the concrete at the cracked section is small. As concrete cohesive stresses in the fictitious cracks are tensile, the small area of the fictitious cracks is needed, and the depth of the fictitious cracks is also small. In these cases, the neutral axis of the cracked section hardly changes, and the section inertia is almost constant, as shown in Figs. 7(b) and 7(c). Therefore, the depth change of the fictitious cracks is the main reason for the inertia change under the loading.

The phenomenon of the inertia change also can be observed in the south side of the beam B1 and the other beams shown in Fig. 8. It is found that the inertias of the sections adjacent to the cracks also change with the load. Then the inertia average of the north and south sides of each beam is taken as the final section inertia, which is used to assess the beam stiffness and predict the beam deflection. These predicted results are shown in Fig. 9 and compared with the experimental data. The initial deflections in the figure are the permanent residual deflections, which were attributable to concrete shrinkage and creep during the sustained loading. The final deflections are the deflections of the beams subjected to the maximum load in the loading and unloading cycles.

From Fig. 9, it is observed that the predicted results coincide well with the experimental data for all the beams. When the load is small, the deflections are nearly linear to the load, which indicates the stiffness of the test beams coincides with the constant inertias shown in Fig. 7 under the small load. When the load becomes larger, the measured deflections of the beams B1 and B2 exhibit nonlinearity. Compared to the method proposed by Xu et al. (2018), the proposed method in this study can predict these nonlinear deflections more accurately. It is because the former method assumed the stiffness was constant under the loading (Xu et al., 2018), while the proposed method models a fictitious crack ahead of each crack, whose depth changes during the loading. Therefore, the proposed method can simulate the nonlinear displacement under the large load.

By comparing the deflections of the test beams, it is observed that although the deflections of the beams B1 and B2 exhibit obvious nonlinear characteristics with the load, the deflections of the beams B3, B5, and B6 are nearly linear to the load. It is due to the fact that the loads acting on the beam B5 and B6 are relatively small and the fictitious cracks ahead of the cracks in these beams do not change their depth obviously, so the change in the inertias is small. Compared to the beams B1 and B2, the beam B3 possesses a larger number of deep cracks. According to the analysis of Fig. 7, the depth of the fictitious crack ahead of a deep crack changes little under the load. As a result, the neutral axis and inertia hardly change, and the stiffness of the beam B3 possessing so many deep cracks is almost constant during the loading process.

3.2 Experimental Work in This Study

In this experiment, two simply supported beams, denoted G1 and G2, were cast. Their spans are 2.6 m and cross sections are 310 × 200 mm rectangular sections. The reinforcement layout of the beams is shown in Fig. 10. The main longitudinal steel bars in the beams are hot-rolled ribbed bars of 16-mm diameter. The mechanical characteristics of concrete are as follows: mean compressive strength f_{cm} is 38.5 MPa; flexural tensile strength f_{ct} is 2.2 MPa; and elastic modulus E_c is 28 GPa. The elastic modulus of the steel bars is 200 GPa, and the yield stress is 400 MPa.

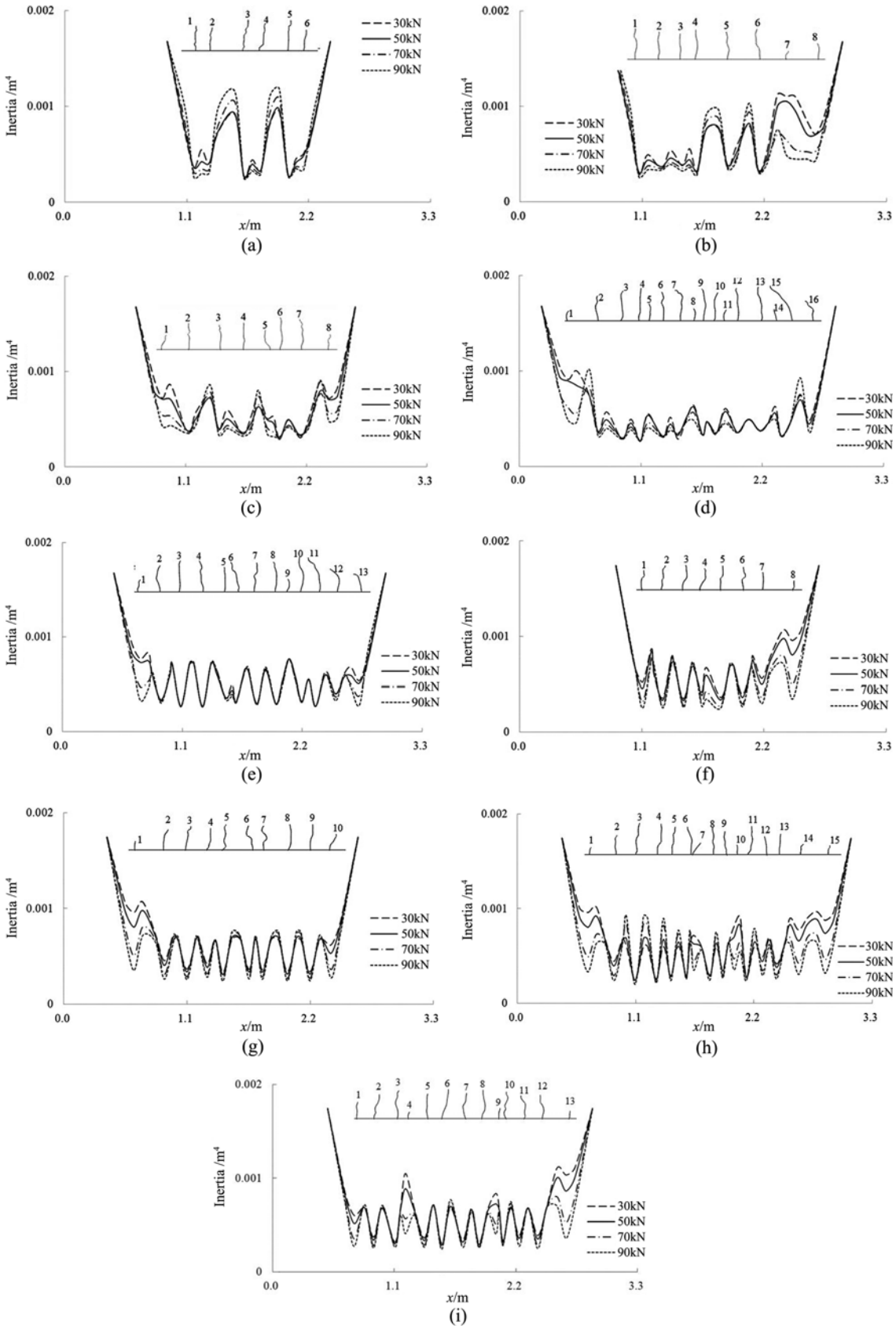

Fig. 8. Section Inertias for the Two Sides of the Test Beams: (a) The South Side of B1, (b) The North Side of B2, (c) The South Side of B2, (d) The North Side of B3, (e) The South Side of B3, (f) The North Side of B5, (g) The South Side of B5, (h) The North Side of B6, (i) The South Side of B6

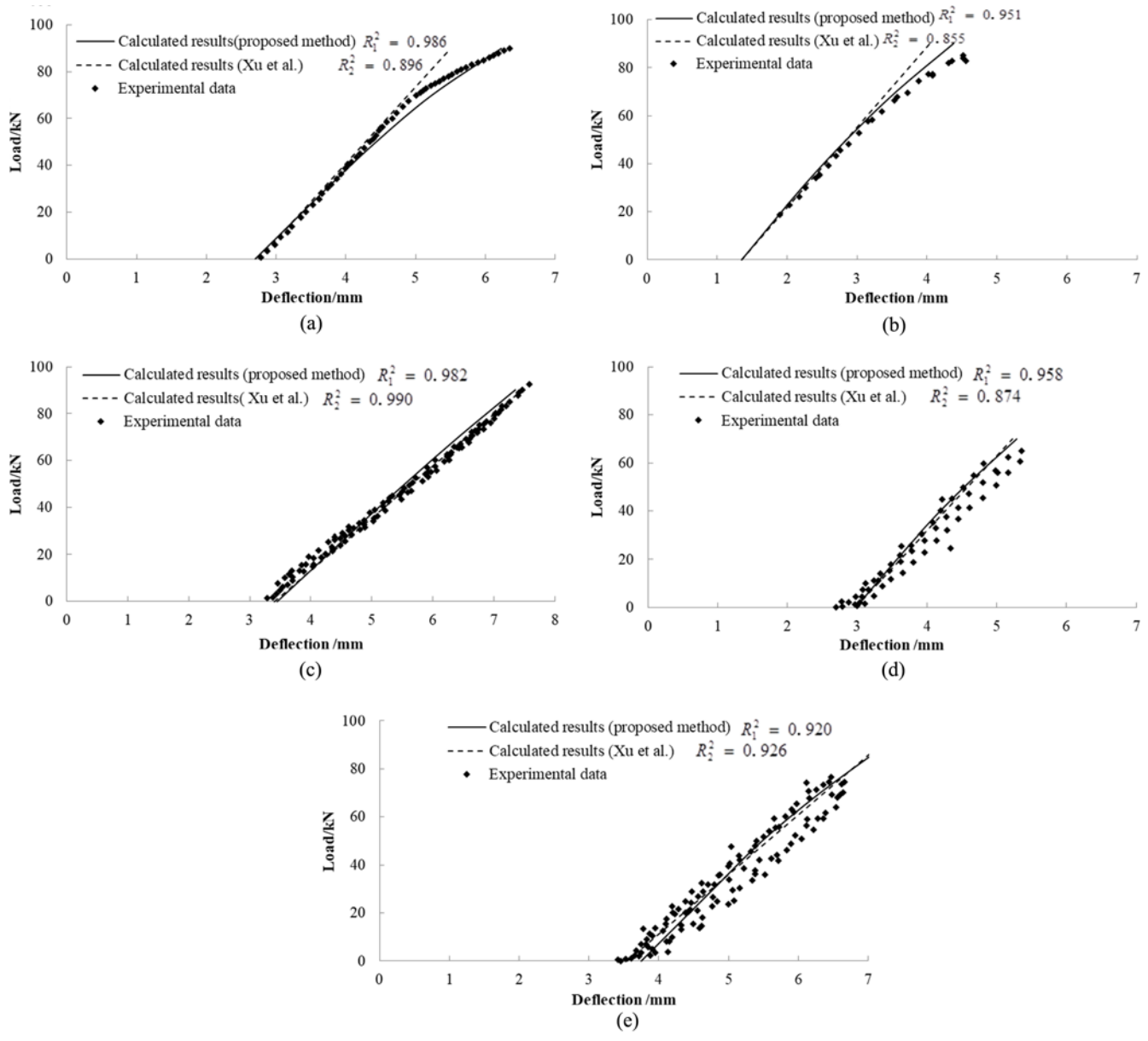

Fig. 9. Comparisons between Calculated and Experimental Displacements of the Test Beams: (a) B1, (b) B2, (c) B3, (d) B5, (e) B6 (R_1 denotes the coefficient of determination for the results calculated by the proposed method, and R_2 is the coefficient for the results by Xu et al. (2018))

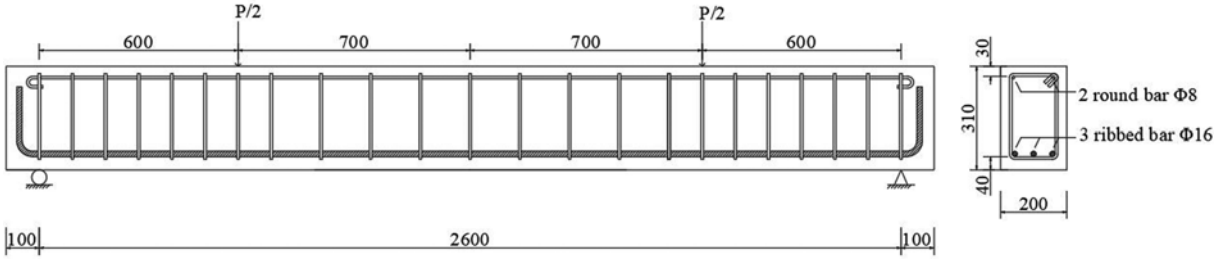

Fig. 10. Layout of the Test Beams with a Span of 2,600 mm (unit: mm)

The test beams had been moist cured for 28 days and then tested in four-point bending for a precracking loading test and repeated loading tests (Fig. 11). In the precracking loading test, the beams were loaded to establish a stabilized cracking pattern, and the peak loads were equal to 70 kN. The cracking pattern was accurately recorded, as shown in Fig. 12. After concrete cracking,

Fig. 11. Loading Procedure of the Test Beams

three loading and unloading cycles were performed, and the maximum loads in the cycles were not bigger than 64 kN. The load value and midspan deflection were measured in each cycle.

The crack spacing is estimated by employing the method suggested by Gribniak et al. (2016), and the section inertias are estimated by using the proposed method from the north and south sides. In the estimation, nonlinear stress distributions are modeled firstly for the cracked sections and key sections near the cracks. Based on the iterative solution of these model, the concrete strains, neutral axis, and the depth of fictitious cracks are obtained. Fig. 13 shows the characteristic change of some cracks in the north side of the beam G1 to illustrate the obtained results.

In these cracks, the depth of the 5th crack is smallest, and the 4th crack is deepest. From Fig. 13(a), it is seen that the fictitious cracks ahead of these cracks increase these depths with the load, and the increase ratio of the 5th crack is largest. These increments will raise the neutral axis of the cracked sections and decrease the section inertias, as shown in Figs. 13(b) and 13(c). Therefore, the section inertias change with load.

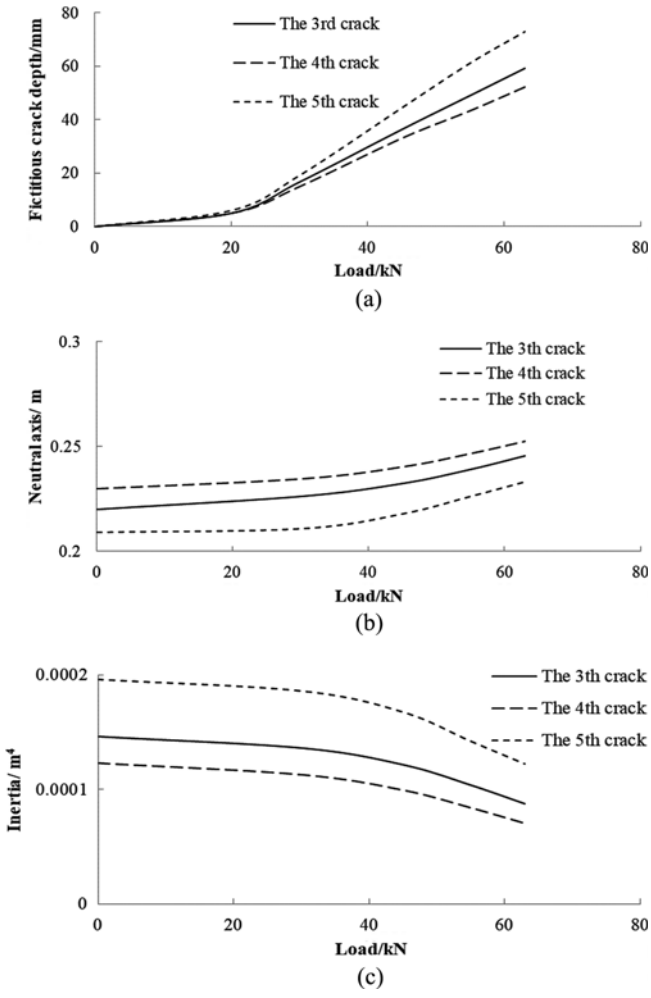

Fig. 13. Characteristics of Cracks in the North Side of the Beam G1: (a) The Fictitious Crack Depths, (b) The Neutral Axis of the Cracked Sections, (c) The Inertias of the Cracked Sections

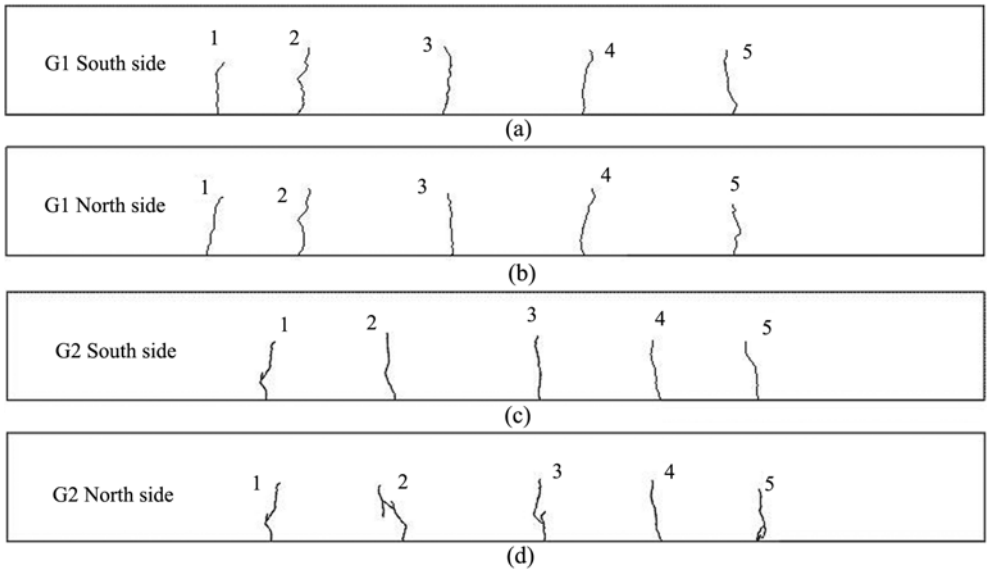

Fig. 12. Cracking Patterns of the Test Beams G1 and G2: (a) G1 South Side, (b) G1 North Side, (c) G2 South Side, (d) G2 North Side

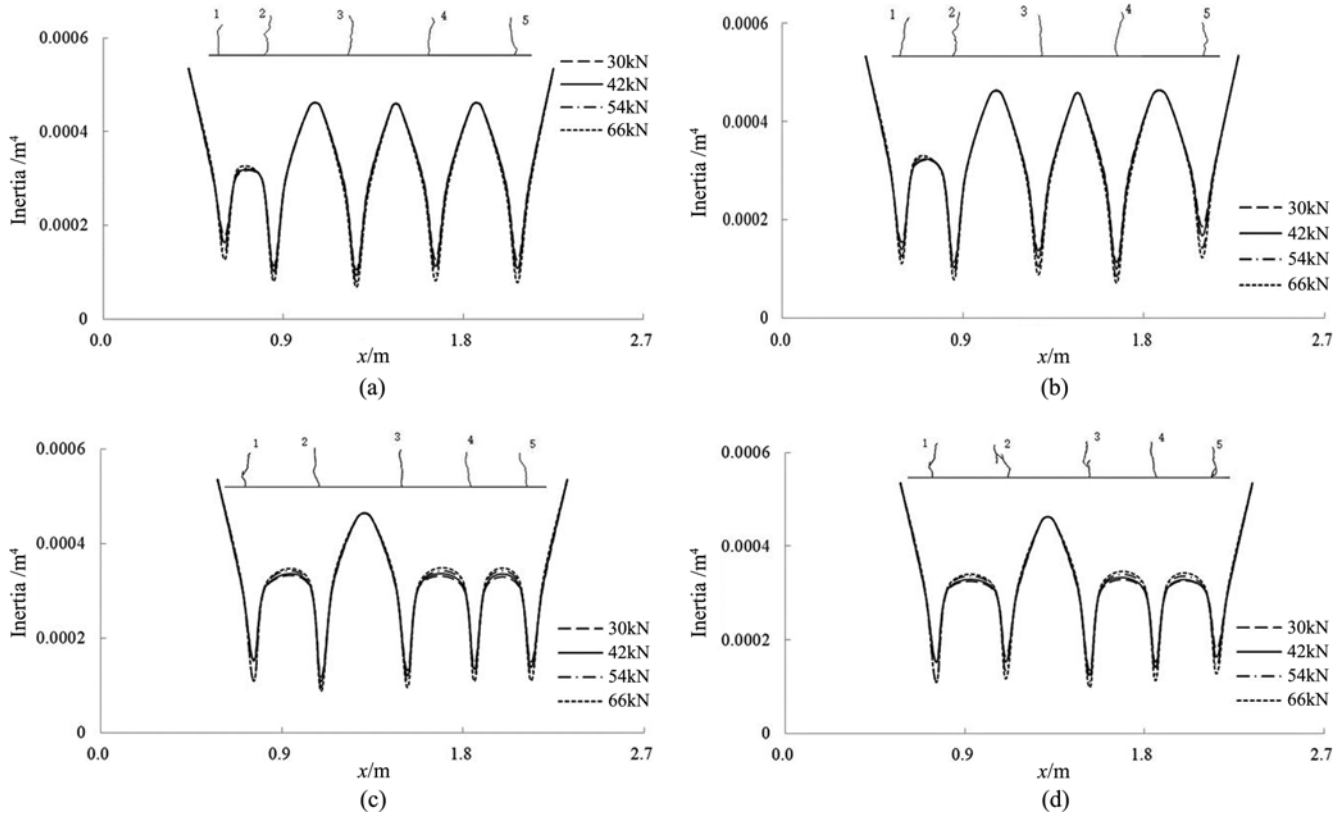

Fig. 14. Section Inertias for the Two Sides of the Test Beams G1 and G2: (a) The South Side of G1, (b) The North Side of G1, (c) The South Side of G2, (d) The North Side of G2

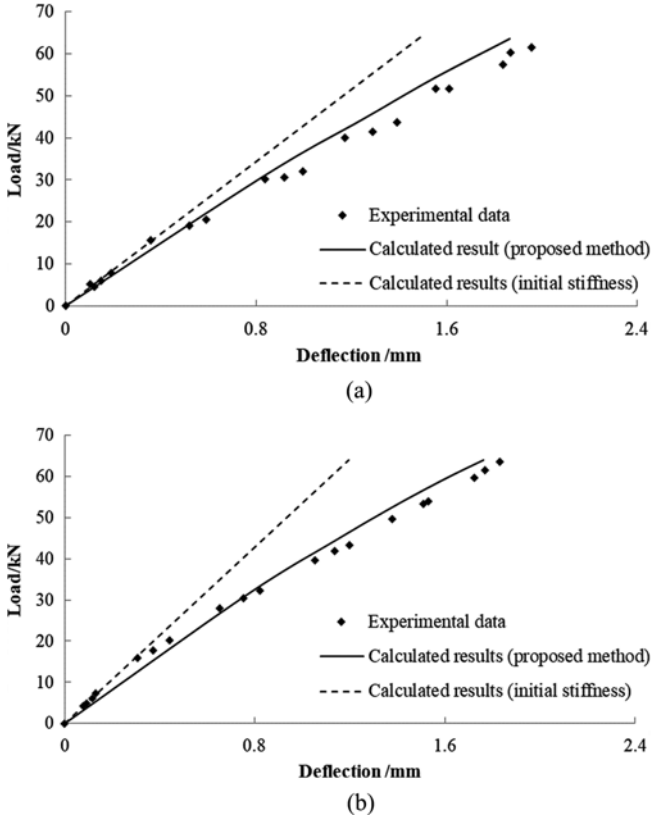

Fig. 15. Comparisons between Calculated and Experimental Displacements of the Test Beams: (a) G1, (b) G2

This phenomenon can be found in the both sides of the beams G1 and G2, as shown in Fig. 14. It is seen that the section inertias reach their local minimums at each crack, and these minimums decrease with the load. Besides, the inertias of sections adjacent to the cracks also change with the load, and the length of the change is large, so the change may obviously affect the global stiffness of the beam.

Then the estimated inertias are used for the stiffness assessment and deflection prediction. The predicted results are shown in Fig. 15 and compared to the experimental data. The deflection is also predicted by using an initial stiffness, which was obtained through dividing the minimum load in each loading cycle by its corresponding deflection measured in the experiment. From the comparison between these results, it is found that while the crack is not propagated, the beam deflection still shows nonlinearity to a certain extent. The proposed method can accurately predict the nonlinear deflection by simulating the change of the inertias of cracked sections and their neighboring sections under the load.

4. Conclusions

A fictitious crack model is introduced into cracked reinforced concrete beams to assess the beam stiffness. Nonlinear concrete stress distributions near cracks are built based on the model. Then the stress of the steel bar at the cracked section is considered as cohesive stress. The concrete and steel stresses are substituted

into the equilibrium equations of forces to solve the concrete stress, and then the section inertias are estimated to assess the beam stiffness. Experimental data from seven concrete beams after cracking are adopted to validate the effectiveness of the proposed method, and the conclusions can be drawn as follows.

1. The fictitious cracks ahead of actual cracks increase their depth with the load, and this increment will raise the neutral axis and decreases the inertia of cracked sections, so the inertias vary with the load due to the change in the depth of fictitious cracks.
2. Through modeling the stress distribution in the regions affected by cracks, the inertias of sections adjacent to the cracks are properly simulated, and their change under the load is taken into account to accurately assess the beam stiffness.
3. The beam deflections measured in the experiments showed nonlinearity under the load, which is accurately predicted using the proposed method. It is because the method has considered the change in the inertias of cracked sections and their neighboring sections under the load.

Acknowledgments

This research was sponsored by the National Natural Science Foundation of China (51508155) and the Fundamental Research Funds for the Center Universities (2017B12314).

Nomenclature

A_c = Area of concrete
A_{ca} = Concrete area above the fictitious crack
A_{cb} = Areas of the parts below the inflection point
A_{cf} = Area between the tips of the fictitious and actual cracks
A_{cu} = Areas of the parts above the inflection point
a_f = Depth of the fictitious crack
A_t = Area of steel bars
a_0 = Initial depth of the crack
b = Width of a beam
c = Thickness of concrete cover
d_t = Distance from the steel centroid to the beam bottom
D_s = Diameter of reinforcing bar
E_c = Concrete elastic modulus
$\mathbf{F}$ = External load vector
f_{ct} = Flexural tensile strength of concrete
f_{ctm} = Mean tensile strength of concrete
f_y = Yield stress of the steel bars
h = Height of a beam
I_0 = Section inertia unaffected by cracks, including the steel contribution
I_{eq} = Inertias of studied sections
I_f = Fitted curve of inertias
$\mathbf{K}_b$ = Global stiffness matrix
$\mathbf{K}_{le}$ = Local stiffness matrix
L = Span of a beam
l_{me} = Element length
l_r = Length of the effect region
l_s = Spacing between two adjacent cracks
l_{sl} = Left crack spacings
l_{sr} = Right crack spacings
l_t = Transfer length
w_b = Crack opening displacement at the crack bottom
w_f = Opening displacement of fictitious crack
w_t = Crack opening displacement at the level of the steel
w_0 = Maximum crack opening width
$\mathbf{X}$ = Displacement vector of the beam
y_n = Y-axis coordinate of neutral axis
ε_{ct} = Concrete strain at the steel level
ε_{ct0} = Concrete strain at the steel level at the sections unaffected by cracks
ε_t = Strain of steel
ε_{tc} = Steel strain at the cracked section
ε_{t0} = Steel strain at the sections unaffected by cracks
$\Delta\varepsilon(x)$ = $\varepsilon_t - \varepsilon_{ct}$
η = Parameter denoting the nonlinear distribution
ρ_{ef} = Effective reinforcement ratio
σ_c = Concrete stress
σ_{cb0} = Bottom strain of sections unaffected by cracks
σ_{ct} = Concrete stress at the beam top
σ_{ctp} = Ctress at the crack tip
σ_t = Stress of the steel bar
σ_w = Cohesive stresses of the concrete
τ_{bms} = Bond strength between steel and concrete

ORCID

Chunyu Fu http://orcid.org/0000-0001-6865-9790
Yin Zhu http://orcid.org/0000-0002-5565-6133
Dawei Tong http://orcid.org/0000-0003-2765-9406

References

Bischoff PH (2005) Reevaluation of deflection prediction for concrete beams reinforced with steel and fiber reinforced polymer bars. *Journal of Structural Engineering* 131(5):752-767, DOI: 10.1061/(ASCE)0733-9445(2005)131:5(752)

Branson DE (1965) Instantaneous and time dependent deflections of simple and continuous reinforced concrete beams. HPR Report No. 7, Alabama Highway Department Bureau of Public Roads, Montgomery, AL, USA

Castel A, Gilbert RI, Ranzi G (2014) Instantaneous stiffness of cracked reinforced concrete including steel-concrete interface damage and long-term effects. *Journal of Structural Engineering* 140(6):1-9, DOI: 10.1061/(ASCE)ST.1943-541X.0000954

Castel A, Vidal T, François R (2012) Finite-element modeling to calculate the overall stiffness of cracked reinforced concrete beams. *Journal of Structural Engineering* 138(8):889-898, DOI: 10.1061/(ASCE)ST.1943-541X.0000520

CEB-FIP (2012) CEB-FIP model code 2010. Thomas Telford, Lausanne, Switzerland, 232-281

Choubey RK, Kumar S, Rao MC (2016) Modeling of fracture parameters for crack propagation in recycled aggregate concrete. *Construction and Building Materials* 106:168-178, DOI: 10.1016/j.conbuildmat.2015.12.101

Fayyad TM, Lees JM (2018) Integrated fracture-based model formulation for RC crack analysis. *Journal of Structural Engineering* 144(7): 04018083, DOI: 10.1061/(ASCE)ST.1943-541X.0002058

François R, Castel A, Vidal T (2006) A finite macro-element for corroded reinforced concrete. *Material Structures* 39:571-584, DOI: 10.1617/s11527-006-9096-x

Gilbert RI (2007) Tension stiffening in lightly reinforced concrete slabs. *Journal of Structural Engineering* 133(6):899-903, DOI: 10.1061/(ASCE)0733-9445(2007)133:6(899)

Gribniak V, Caldentey AP, Kaklauskas G, Rimkus A, Sokolov A (2016) Effect of arrangement of tensile reinforcement on flexural stiffness and cracking. *Engineering Structures* 124(6):418-428, DOI: 10.1016/j.engstruct.2016.06.026

Gribniak V, Cervenka V, Kaklauskas G (2013) Deflection prediction of reinforced concrete beams by design codes and computer simulation. *Engineering Structures* 56(6):2175-2186, DOI: 10.1016/j.engstruct.2013.08.045

Hillerborg A, Modeer M, Petersson PE (1976) Analysis of crack formation and crack growth in concrete by means of fracture mechanics and finite elements. *Cement and Concrete Research* 6(6):773-782, DOI: 10.1016/0008-8846(76)90007-7

Hu X, Duan K (2010) Mechanism behind the size effect phenomenon. *Journal of Structural Engineering* 136(1):60-68, DOI: 10.1061/(ASCE)EM.1943-7889.0000070

Kalkan I, Lee JH (2013) Effect of shrinkage restraint on deflections of reinforced self-compacting concrete beams. *KSCE Journal of Civil Engineering* 17(7):1672-1681, DOI: 10.1007/s12205-013-1007-4

Logan DL (2007) A first course in the finite element method. Thomson, Toronto, Canada, 131-212

Murray A, Castel A, Gilbert RI, Chang ZT (2016) Time-dependent changes in the instantaneous stiffness of reinforced concrete beams. *Engineering Structures* 126:641-651, DOI: 10.1016/j.engstruct.2016.08.025

Qing L, Cheng Y (2018) The fracture extreme theory for determining the effective fracture toughness and tensile strength of concrete. *Theoretical and Applied Fracture Mechanics* 96:461-467, DOI: 10.1016/j.tafmec.2018.06.009

Reinhardt HW, Cornelissen HAW, Hordijk DA (1986) Tensile tests and failure analysis of concrete. *Journal of Structural Engineering* 112(11): 2462-2477, DOI: 10.1061/(ASCE)0733-9445(1986)112:11(2462)

Wittmann FH (1983) Fracture mechanics of concrete. Elsevier, Amsterdam, Netherlands, 117-135

Wu Z, Yang S, Hu X, Zheng J (2006) An analytical model to predict the effective fracture toughness of concrete for three-point bending notched beams. *Engineering Fracture Mechanics* 73:2166-2191, DOI: 10.1016/j.engfracmech.2006.04.001

Xu T, Zhu L, Castel A, Gilbert RI (2018) Assessing immediate and time-dependent instantaneous stiffness of cracked reinforced concrete beams using residual cracks. *Journal of Structural Engineering* 144(4):1-12, DOI: 10.1061/(ASCE)ST.1943-541X.0002009